AGU PUBLICATIONS

Geochemistry, Geophysics, Geosystems

TECHNICAL REPORTS: METHODS

10.1002/2016GC006615

Key Points:
- A high-sensitivity spinner magnetometer using magneto-impedance (MI) sensor was developed
- A wide dynamic range from 10^{-10} to 10^{-4} Am^2 and a resolution of 10^{-11} Am^2 were achieved
- It is capable of measuring higher-order harmonics, useful for the quantification of inhomogeneous magnetization of samples

Correspondence to:
K. Kodama,
kdma@kochi-u.ac.jp

Citation:
Kodama, K. (2017), High-sensitivity multifunctional spinner magnetometer using a magneto-impedance sensor, *Geochem. Geophys. Geosyst.*, *18*, 434–444, doi:10.1002/2016GC006615.

Received 30 AUG 2016
Accepted 15 DEC 2016
Accepted article online 29 DEC 2016
Published online 17 JAN 2017

High-sensitivity multifunctional spinner magnetometer using a magneto-impedance sensor

Kazuto Kodama[1]

[1]Center for Advanced Marine Core Research, Kochi University, Kochi, Japan

Abstract A novel spinner magnetometer was developed with a wide dynamic range from 10^{-10} to 10^{-4} Am^2 and a resolution of 10^{-11} Am^2. High sensitivity was achieved with the use of a magneto-impedance (MI) sensor, which is a compact, sensitive magnetic sensor used industrially. Its slow-spinning rate (5 Hz) and the incorporation of a unique mechanism for adjusting the spacing between the sensing unit and the spinning axis allows the measurement of fragile samples sized 10–50 mm. The sensor configuration, in which a pair of MI sensors is connected in opposite serial, along with an amplification circuit with a programmable low-pass filter, reduces the problems of external noise and sensor drift. The signal, with reference to the spinning frequency, is detected with a lock-in amplifier. The MI spinner has two selectable measurement modes: the fundamental mode (F mode) and the harmonic mode (H mode). Measurements in the F mode detect signals of the fundamental frequency (5 Hz), in the same way as conventional spinner magnetometers. In the H mode, the second (10 Hz) and the third (15 Hz) harmonic components are measured, in addition to the fundamental component. Tests in the H mode were performed using a small coil and a natural sample to simulate dipoles with various degrees of offset. The results revealed that the magnitude of the fundamental component of the offset dipole was systematically larger (by several percent) than that of the nonoffset dipole. These findings suggest that this novel MI spinner will be useful in estimating the inhomogeneity of the magnetization of a sample that can equivalently be described by an offset dipole.

1. Introduction

Magnetometers for paleomagnetism and rock magnetism are generally classified into three categories in terms of sensitivity and signal detection: vibrating sample magnetometers (VSM), spinner magnetometers (SPM), and superconducting rock magnetometers (SRM) [*Collinson*, 1983]. Depending on the sensitivity and the subject of research, an appropriate magnetometer is chosen for the routine measurement of a number of samples or characterization of the magnetic properties for intensive rock magnetic analyses of selected samples. Magnetic sensors employed by these magnetometers include inductive coils, flux-gate sensors, and superconducting quantum interference devices. Inductive coils have mainly been used for VSM because they can detect the induced magnetization of a sample oscillating synchronously with the vibration frequency in a steady field, and are thus most suitable for obtaining hysteresis curves. Because inductive signals increase in proportion to the frequency of an oscillating sample, inductive coils remain in use as magnetic sensors in high spinning SPM. However, the high spinning speed, as much as tens of rotations per second, requires a complicated rotation mechanism, making it difficult to measure fragile or large samples. Instead, flux-gate sensors provide moderate sensitivity without strong frequency dependence, and thus have been used for SPMs with relatively slow-spinning speeds. The use of a phase-lock loop with reference to the rotation frequency, along with digital signal processing, helps to greatly increase the sensitivity [*Molyneux*, 1971]. However, it is often time consuming to stack a number of data to achieve a desired signal-to-noise ratio (SNR) and to reposition a sample about three perpendicular axes for averaging. Consequently, it appears that the outstanding sensitivity and rapid measurement time of SRM make it a de facto standard in paleomagnetism and rock magnetism.

However, in light of both maintenance and cost, the development of a novel type of compact, cost-effective SPM, with a sensitivity high enough to measure samples that would have necessitated the use of an SRM, would seem to be worthwhile. In addition, recent advances in the field of spintronics, a

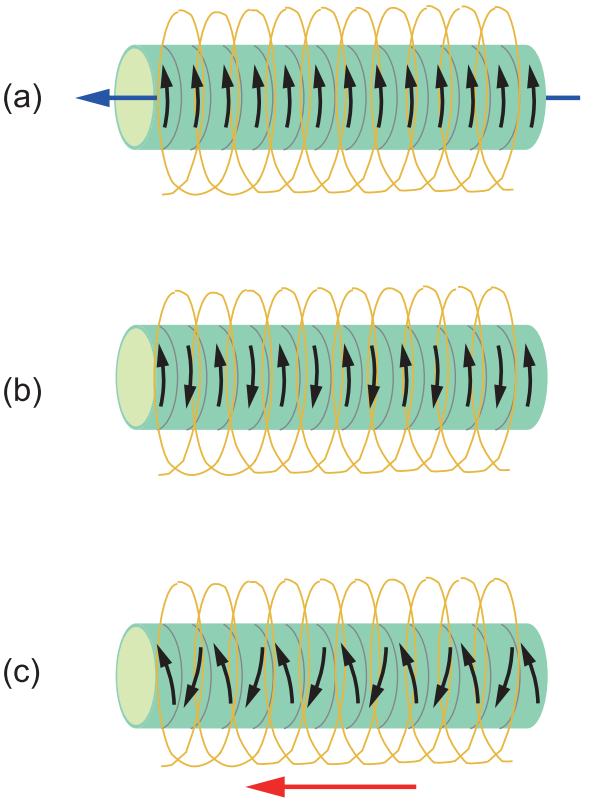

Figure 1. Outline and operating principle of MI sensor. (a) Applying a pulsed current to the wire (blue arrow), the spin moments in the circular domains at the surface are directed normal to the wire. (b) In the absence of an external field, the spin magnetic moments are directed antiparallel to each other. (c) In the presence of an axial external field (red arrow), the spin magnetic moments are canted slightly by the axial field. A greater change in impedance in Figure 1c is sensed by the pick-up coil surrounding the wire.

cutting-edge technology based on quantum mechanics and microelectronics [e.g., *Bandyopadhyay and Cahay*, 2015], have produced various types of new magnetic sensors that are now commercially available [e.g., *Park*, 2015]. One of these is a magneto-impedance (MI) sensor that was developed by a Japanese research group [*Mohri et al*., 1995]. To date, a few versions of the MI sensor have been produced with different sizes and sensitivities depending on the devices that incorporate them [*Mohri et al*., 2010; *Uchiyama et al*., 2012]. The sensitivity, or the lowest measurable value, is variable, generally ranging from 0.1 to 10 nT. For example, the smallest device has dimensions of 1 × 1 × 2 mm and is used mainly for the digital compass in smartphones. Even these small MI chips incorporate a three-axis MI sensor, allowing measurements of the geomagnetic field direction to an accuracy of 0.2° [*Mohri and Honkura*, 2007]. An application of an earlier version of the MI sensor to rock magnetism was undertaken by *Uehara and Nakamura* [2007], utilizing it as the sensor of a magnetic scanner for two-dimensional mapping of the flat surface of a sample. Other investigations reported that flux-gate sensor is comparable to the MI sensors in terms of sensitivity and noise [*Dufay et al*., 2013]. However, the recent commercial MI sensors, which are small-sized, low-cost, low power consumption, and more sensitive than the earlier versions, expand the potential for the sensor of magnetometers for rock magnetic investigations. The current study introduces an MI spinner magnetometer, or MI SPM, the application of the MI sensor in an instrument used to measure the remanent magnetization vector of natural samples by repositioning about only two perpendicular axes. Its design, features, and advantages over the previous SPMs are described in the following section.

2. Principles, Methods, and Hardware

Figure 1 provides an outline of the MI sensor used in this study. The sensor consists of a high-permeability, amorphous wire such as FeCoSiB, and a surrounding pick-up coil [*Uchiyama et al*., 2012]. This surface anisotropy produces an enhanced skin effect on the application of a pulsed current to the wire, and the spin magnetic moments in the circular domains at the surface are directed normal to the wire (Figure 1a). On removal of the pulsed current, in the absence of an external field, the spin moments in the neighboring domains are relaxed and directed antiparallel to each other (Figure 1b). In the presence of an axial external field, the spin moments are canted slightly by the axial field (Figure 1c). These characteristic behaviors of the spin moment change the impedance (or permeability) of the wire, which is sensed by the pick-up coil surrounding it. This results in a greater change in impedance in Figure 1c than in the field-free case (Figure 1b), generating a larger induced voltage in the pick-up coil. The induced voltage is proportional to the intensity of the external field, and is practically detected as the DC voltage by the amplitude modulation when a high-frequency (>1 MHz) current pulse is applied to the wire. The circuits for processing these pulsed signals, as well as the wire and pickup coil, are assembled together in a small packaging board.

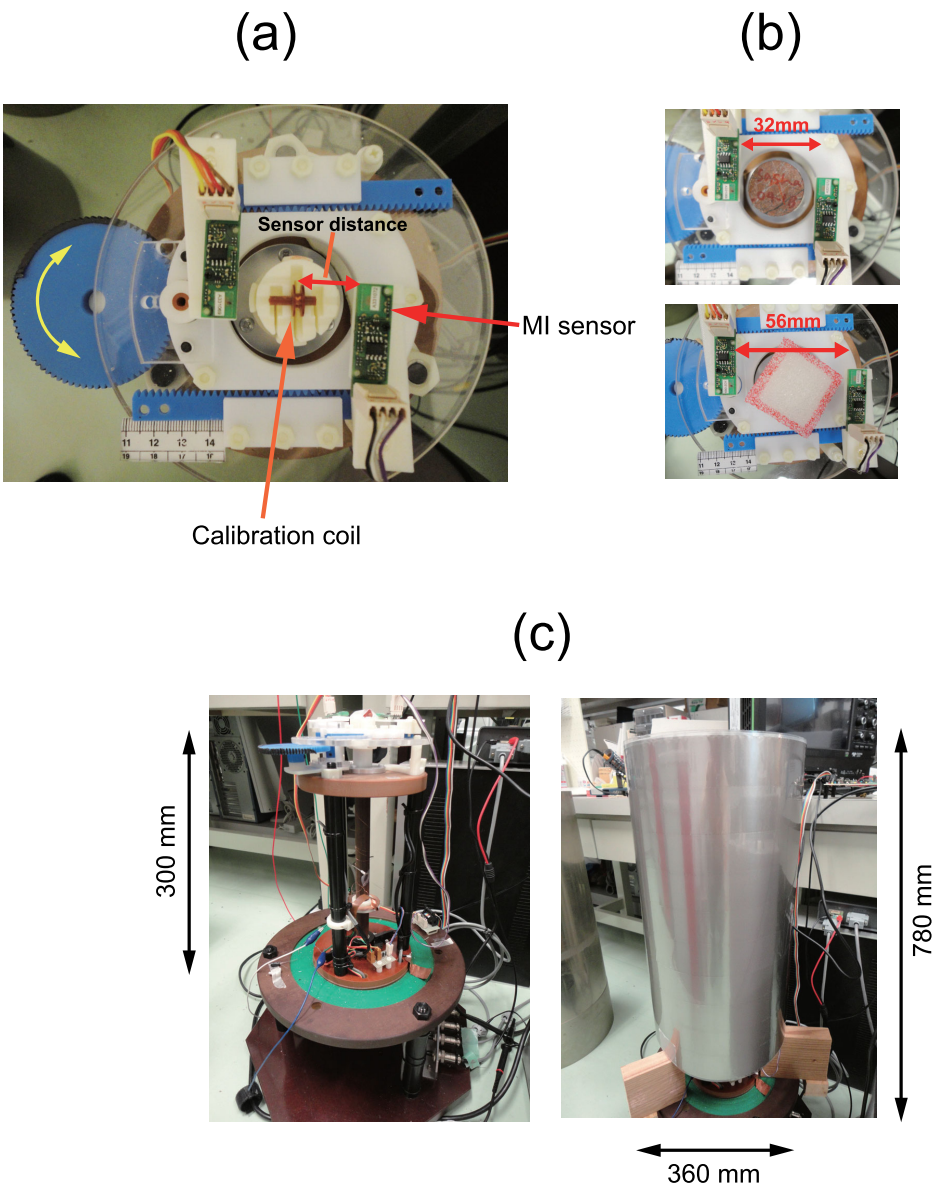

Figure 2. (a) Top view of the MI spinner showing the sensor configuration and the sample holder in the middle. (b) By turning the gear wheel (blue) on the left side, the spacing between the sensing units of the two packaging board can be changed continuously from (top) 32 mm to (bottom) 56 mm. (c) Whole system (right) with a magnetic shield case and (left) without it. The sample-sensor region is located 300 mm from the bottom of the case.

The MI sensor employed in this study is the most sensitive sensor that is commercially available (Model MI-CB-1DH; Aichi Steel Co., Aichi, Japan) and is referred to as the "nano-Tesla MI sensor." It is used mainly for inspecting small magnetic particles in fabrics and foods. The sensor configuration of the MI spinner takes on a symmetrical arrangement (Figure 2a), where a pair of MI sensors is connected in opposite series so that external noise and the ambient field inside the magnetic shield are canceled. The difference in the sensitivity between these two sensors is within 1%. Such a sensor layout, along with the signal processing circuit consisting of a high-gain amplification and negative feedback, can improve the sensitivity required from magnetometers used in medical applications [*Uchiyama et al*., 2012]. Another advantage of this sensor configuration, a type of gradiometer configuration, is that it can attenuate the even-order harmonic waves in the output signals. For example, given the angular frequency, ω, of a rotating sample and neglecting the harmonics with orders >3, the output from one of the paired sensors contains the three components, C_1, C_2, and C_3, which correspond to the fundamental wave, the second harmonic, and the third harmonic,

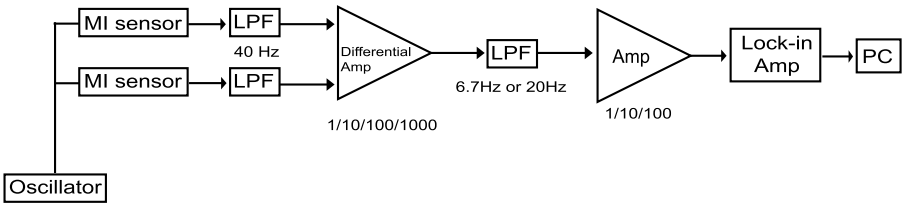

Figure 3. Circuit diagram consisting of low-pass filter (LPF), differential amplifier, and AC amplifier. The selectable cutoff frequency of the second-stage LPF allows measurements of the second (10 Hz) and third (15 Hz) harmonic wave components.

respectively. Consequently, each wave component is represented in the form of $C_1 = A_1\sin(\omega t)$, $C_2 = A_2\sin(2\omega t)$, and $C_3 = A_3\sin(3\omega t)$. Likewise, the output from the other MI sensor 180° apart contains the three corresponding components of the forms following: $A_1\sin(\omega t + \pi) = -C_1$, $A_2\sin(2(\omega t + \pi)) = A_2\sin(2\omega t) = C_2$, and $A_3\sin(3(\omega t + \pi)) = -A_3\sin(3\omega t) = -C_3$. Therefore, differencing the outputs from the paired sensors, the second-order harmonic is eliminated whereas the fundamental wave and the third harmonic are doubled. Thus, employing an appropriate low-pass filter (LPF), the fundamental wave corresponding to the dipole component can be measured more effectively than in a single-sensor configuration.

To adapt the differential MI sensor system for SPM, a specific circuit was built, consisting of LPF, differential amplifier, and AC amplifier (Figure 3). The LPF is a fourth-order Butterworth filter, with the cutoff frequency, f_c, tunable between 1 and 40 Hz, with the precision of 1% (SR-4BL, NF Co., Tokyo, Japan). The output is transferred to a digital lock-in amplifier (LI5655; NF Co., Tokyo, Japan) for lock-in detection using a reference signal of 5 Hz supplied from the optical encoder. The f_c is normally set to 6.7 Hz to detect the fundamental, sinusoidal signal of 5 Hz, referred to herein as the fundamental mode (F mode). Additionally, there is a supplementary mode, the harmonic mode (H mode), with f_c set to 20 Hz, allowing measurements of the second (10 Hz) and third (15 Hz) harmonic wave components. This selectable-mode function was implemented to elucidate the waveform distortion of samples due to either inhomogeneous magnetization or shape irregularities. The waveforms, along with their fast Fourier transform (FFT) spectrum, were monitored with a digital oscilloscope (HDO6104; Teledyne LeCroy, NY, USA).

To achieve a wide dynamic range, a special mechanism was incorporated into the sensor arrangement. This device is a type of rack-and-pinion gear system, with two arms attached to each of the MI sensors (Figure 2a), so that by turning the gear wheel it is possible to change the spacing between the spinning axis and the location of the sensing unit within the packaging board, referred hereafter to the sensor distance (Figure 2a), from the closest (14 mm) to the farthest (37 mm) distance. As a result of the lock-in detection, most of the samples were found to be measurable at a fixed sensor distance of between 17 and 20 mm. Appropriate adjustment was necessary only for extremely weak ($<10^{-9}$ Am^2) or strong ($>10^{-5}$ Am^2) samples. Consequently, in combination with the variable-gain amplifier ($\times$1, 10, 10^2), the overall dynamic range of the SPM reached the sixth order of magnitude, from 10^{-10} to 10^{-4} Am^2. This is equivalent in magnetization per volume, to 10^{-8} to 10^{-2} kA/m (or emu/cm^3) for standard 1 inch cylinder samples or 10 cm^3 cubes. The spinning mechanism in the vertical magnetic shielding (Figure 2c) was diverted from that used in a conventional SPM (SMD-88, Natsuhara-Giken, Osaka, Japan). The vertical system is preferable to the horizontal one, because it proves easy access to the measuring place for changing and repositioning samples, and to the translation gear for adjusting the sensor distance.

3. Results

3.1. Calibration

Calibration was performed in the F mode using a set of synthetic samples and a small dipole-simulating coil. The coil was 2 mm long, 4 mm in diameter, and was wound 100 times in two layers using 0.1 mm wire on a bakelite bobbin (Figure 4a). The coil was connected to an external current supply via a brush attached to the spinning axis. Each of the synthetic samples was made of ferrite, had a size of 2 mm $\times$ 1 mm, had a known axial magnetization, and was molded by resin and placed at the center of a plastic 1 inch cube. The magnetic moment of these synthetic samples was measured beforehand with an SRM (2G Model 765), ranging over 4 orders of magnitude from 10^{-9} to 10^{-6} Am^2. The magnetic moments were then measured

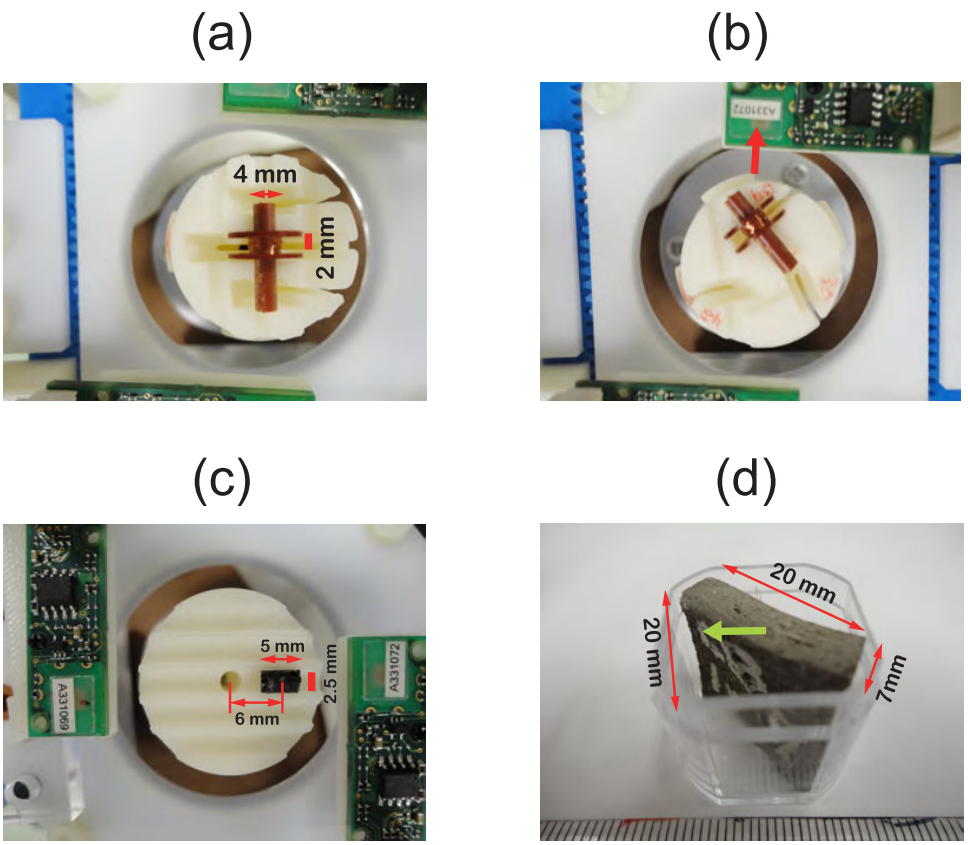

Figure 4. (a) Dipole-simulating coil (4 × 2 mm) placed at the center of the sample holder. (b) The same coil with the offset of 4 mm away from the spinning axis in the orientation 30° CCW with respect to the sensing direction of the MI sensor (red arrow). (c) A mini-core sample of basalt (5 mm long, 2.5 mm in diameter, weighing 87 mg), with the axial ARM of 5.3×10^{-6} Am^2, placed on a special holder for simulating a dipole with the offset of 6 mm. The amount of the offset was varied by changing the distance from the spinning axis to the middle of the mini-core. (d) A fragment of a Japanese porcelain sample (20 × 20 × 7 mm), with the ARM in the designated direction (green arrow), in a plastic 1 inch cube.

by the MI spinner to create a calibration curve used to convert the output as a voltage to the magnetic moment. Using the calibration constant (= 2.08×10^{-9} Am^2/mV), the current supplied to the coil was converted into the magnetic moment. These calibration curves are shown in Figure 5, and were created at a sensor distance of 17 mm. Calibrations using the test coil were repeated at various sensor distances, and the results are shown in Figure 6a demonstrating straight lines with no distinctive effect of the sensor distance on the accuracy of the fitting. Figure 6b plots the gradients of the fitted lines at the five different sensor distances versus the inverse cube of the sensor distance, with the well-fitted straight line suggesting the dominance of the dipole contribution.

Concerning the calibration in the F mode, it is necessary to evaluate how the f_c (=6.7 Hz) of the LPF affects the gain at 5 Hz. For the fourth-order Butterworth LPF employed in this study, the gain at 5 Hz is slightly smaller than unity, or 0.96. This means that the fundamental component measured in the F mode is consistently attenuated by approximately 4% than measured in the H mode. It is to be noted that the aforementioned calibration factor (= 2.08×10^{-9} Am^2/mV) calculated using the small coil already compensated for the attenuation. However, when converting the amplitude of the waveforms in the H mode to the magnetic moment, it is necessary to employ the calibration factor corrected for the 4% discrepancy between the F mode and the H mode.

3.2. Measurement in the H Mode

The calibration coil was also used to assess the effect of the offset dipole on the magnetization measured by SPM. A series of measurements were made in the H mode by varying factors such as the supplied current, the amount of offset, and the orientation of the offset dipole. In the experiments, the coil was settled

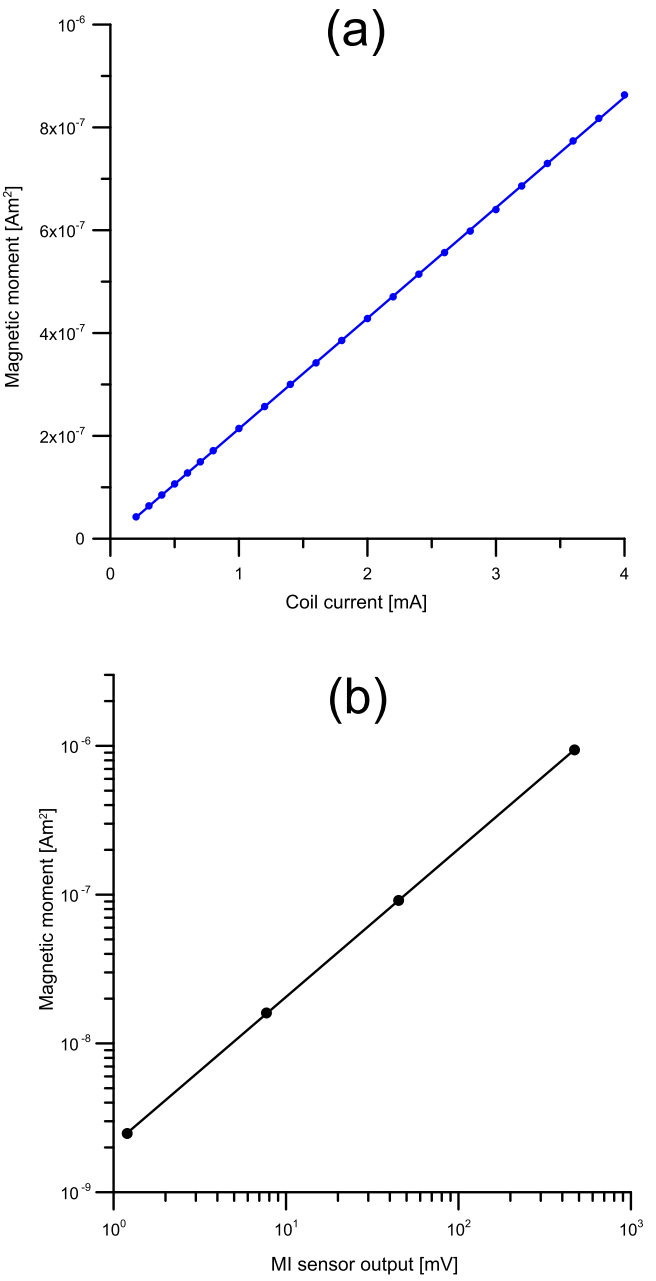

Figure 5. (a) Magnetic moment (Am^2) versus supplied current (mA) at the sensor distance of 17 mm. (b) Magnetic moment (Am^2) versus MI sensor output ranging in the three orders of magnitudes in mV.

in a plastic container with notches at different orientations (Figure 4b). The offset was 3 mm, or 18% of the sensor distance of 17 mm, in three different orientations (30° and 60°) with respect to the reference direction. The signal waveforms that were expected to contain harmonic components were transferred to the lock-in amplifier so that only the fundamental component was detected. For comparison, measurements in the F mode were made with the coil using the same offset arrangements. The resulting waveforms and associated FFT spectrum are provided in Figure 7. It is clear that the waveforms in the H mode are more or less skewed, showing various degrees of inclusion of the harmonic components. This is more clearly apparent in the FFT spectrum, with three prominent peaks below the f_c (=20 Hz), which correspond to the fundamental component (=5 Hz), the second harmonic (10 Hz), and the third harmonic (15 Hz), respectively. Consequently, these peak heights are expected to represent the relative contribution of the three major components in the waveforms of the offset dipole. Notably, the waveforms in the F mode are totally sinusoidal: a clear manifestation of the low-f_c LPF.

In the FFT spectrum in Figure 7, several pronounced peaks corresponding to the even-order harmonics are observed; for example, the peak of the second-order harmonic is notable between the fundamental component and third-order harmonic component. This seems to be contrary to the theoretical expectation described above that the even-order harmonics would be canceled due to the differential configuration of the two sensors. In practice, however, it is hard to achieve the complete cancellation. This is principally because the measurement with the MI sensor is made in close proximity to a sample, meaning that the sensitivity is critical to the sensor distance. Consequently, even if using a pair of MI sensors with identical sensitivity, the complete cancelation of the second-order harmonics would not be realized due to a slight imbalance in the differential configuration of the sensors.

The effect of the offset was assessed in terms of the amplitude of the fundamental wave and the harmonics versus the amount of the offset. The mini-core sample (Figure 4c) was set at five different spacing (3, 4, 6, 8, and 10 mm) between the center of the container and the middle of the mini-core. And, it was measured with the MI spinner at the sensor distance of 14 mm, and was also measured with another SPM (SMD-88)

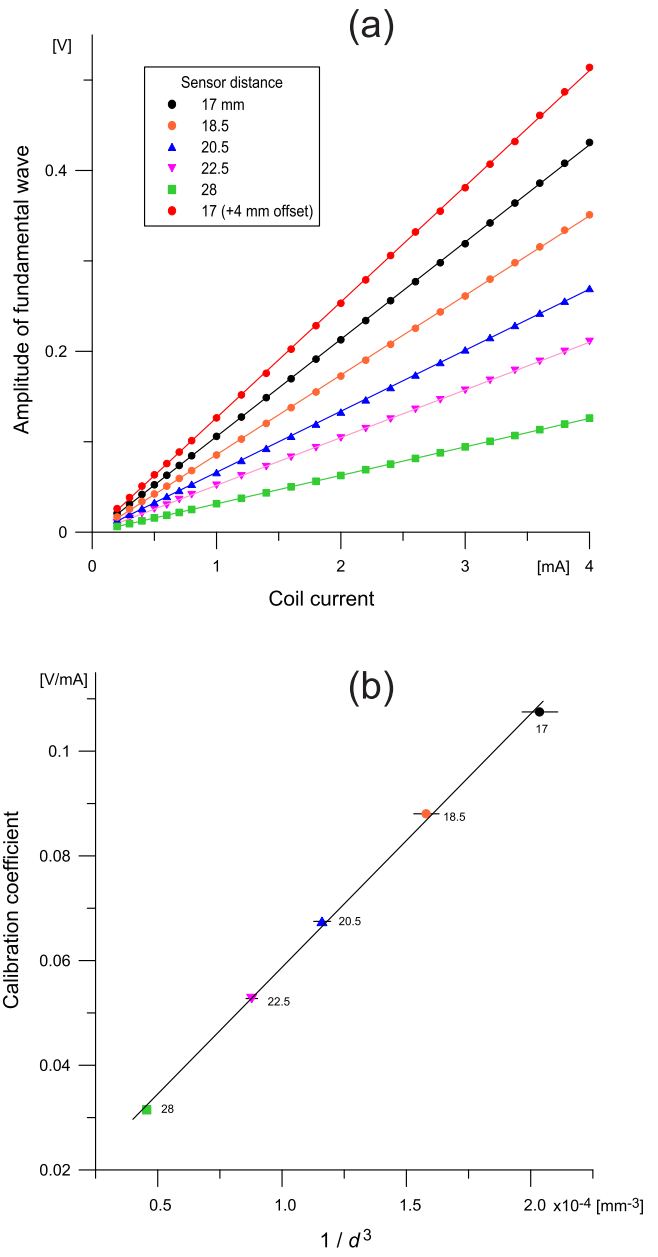

Figure 6. (a) Amplitude of fundamental wave component versus current supplied to the nonoffset calibration coil measured at different sensor distances. The result from the offset coils (4 mm off the spin axis), measured at the sensor distance of 17 mm, is added for comparison (red circles). Measurements at each current step were made for the period ~10 s (50 rotations), with the errors < 1% smaller than the size of the symbols. (b) Gradients (calibration constants) of the fitted lines in (a) versus d^{-3} (d = sensor distance). Symbols are the same as in (a), with the values of d attached to each point. Error bars are added provided the 0.5 mm margin of error for d.

employing a ring-core, flux-gate sensor with a radius of 30 mm. Figure 8 provides plots of the amplitude of both the fundamental wave and the third harmonic wave versus the offset normalized to the sensor distance. For comparison, a similar plot was provided for the results from the MI SPM using the test coil at two different offsets. The amplitudes in these plots, without exception, increased with the amount of the offset.

The measured data in Figure 8 were fitted with two different curves; one is a quadratic curve and the other is a polynomial curve consisting of the second- to forth-order terms. It appears that the single quadratic curve showed an appropriate fitting for the normalized offset $<\sim 0.3$, but over the entire range the polynomial curve showed excellent fitting. It is reasonable that the inclusion of the higher-order terms results in better fitting, but, physically, it suggests that the contribution from the higher-order harmonic components could be represented in the form of a nonlinear function of the offset distance.

The measurements by the conventional SPM also demonstrated a similar increasing curve, associated with relatively large errors than those by the MI SPM. These errors were generated by averaging the six measurements about three perpendicular axes. The smaller increase rate in this SPM is most likely due to its high-order LPF and the large sensor distance for isolating only the fundamental wave component. However, the systematic increase with the offset is contrary to the expectation that, given the same sample with the same magnetic moment, the magnetization measured for the offset and nonoffset samples will be identical. This finding suggests that the intensity of magnetization, measured with conventional SPMs in the same way as with the MI spinner, may include a systematic bias, particularly when samples contain a large amount of harmonic component that can be represented by an offset dipole. The systematic relationship between the amplitude and the offset could be explained quantitatively in terms of the dipole and higher-order multipoles and their varying contributions dependent of the amount of offset.

The data obtained in the F mode in Figure 6a showed a difference of ~5% between the offset and nonoffset coil, whereas those measured in the H mode in Figure 8b at the normalized offset corresponding to the

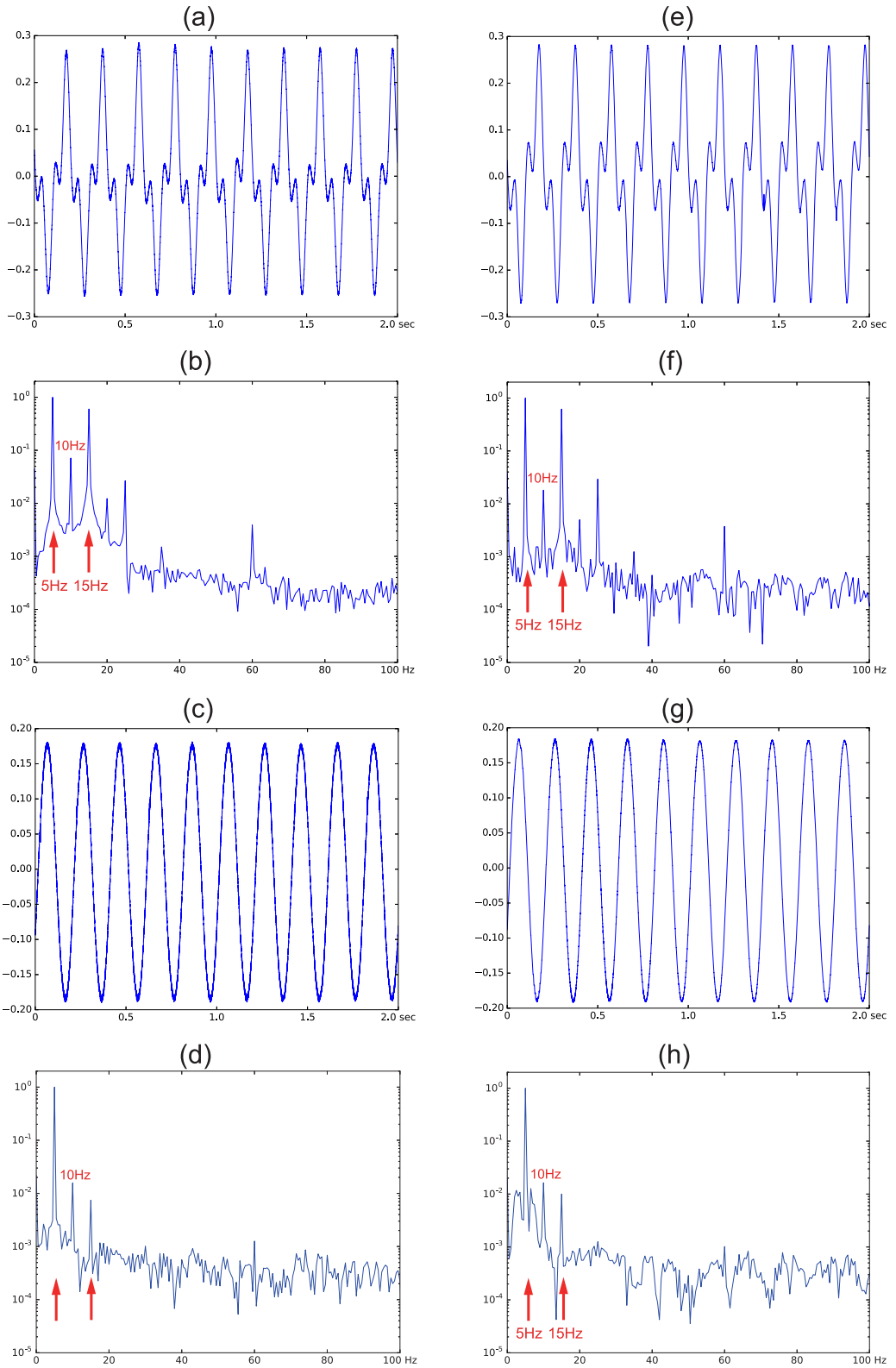

Figure 7. Waveforms and their corresponding FFT spectrum, recorded for 2 s using the test coil with the supplied current of 2 mA in two different orientations, (a–d) 30° and (e–h) 60°. The waveforms were measured in the (a, e) H mode and (c, g) F mode.

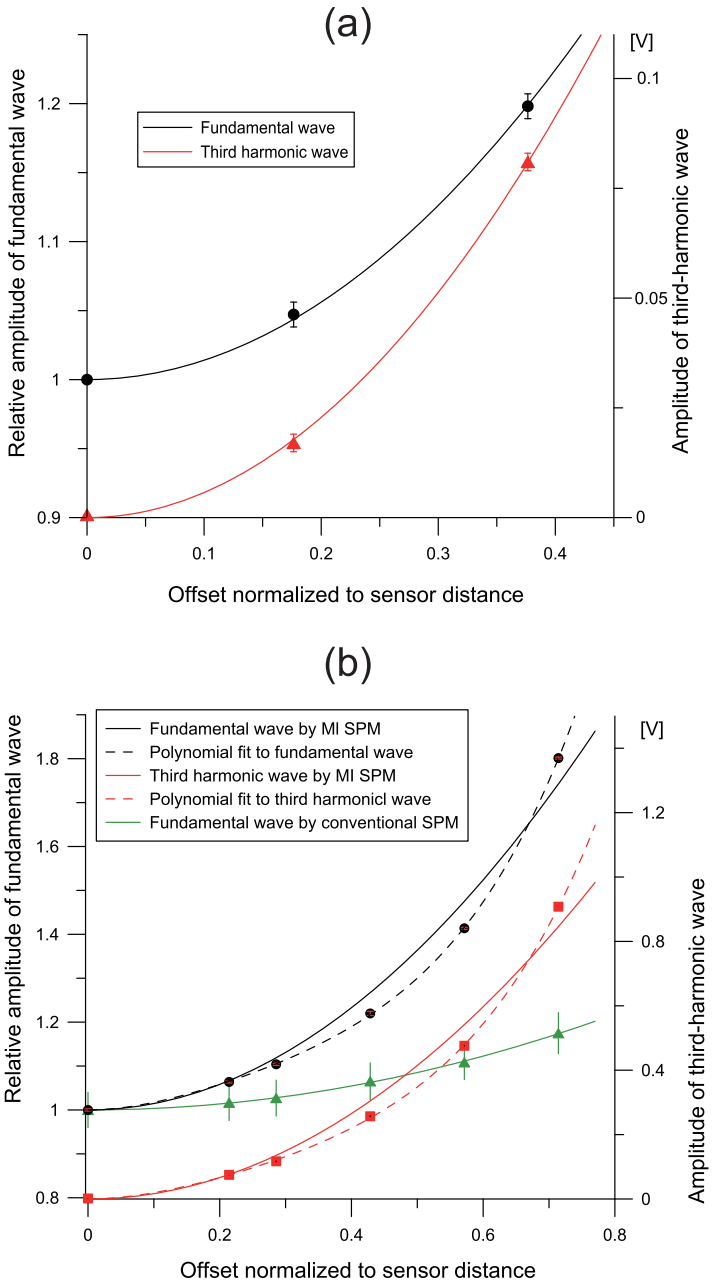

Figure 8. Amplitudes of the fundamental wave and the third harmonic wave versus the offset normalized to the sensor distance. The amplitude of the fundamental wave is normalized to the value at the nonoffset position (*y* axis to the left). The amplitude of the harmonic wave is given in volt (*y* axis to the right). (a) Calibration coil at no offset and two different offset positions, with quadratic curve fittings. (b) Mini-core sample of basalt at no offset and five offset positions with the use of the holder in Figure 4c, measured by both the MI SPM and the conventional SPM. Fitted with a quadratic curve (solid lines) and with a polynomial curve including the second- to forth-order terms (dotted lines).

sample-sensor configuration in Figure 6a indicated a slightly larger difference of ∼8%. This discrepancy between the F mode and the H mode is most likely due to the difference in the analog filter gain employed in the two modes. In practice, these discrepancies can be compensated by the calibration constants for converting the measured data to the magnetic moments.

Furthermore, to examine whether the presence of higher-order harmonics may originate, in a similar way to the offset dipole, from the irregularity in shape, the fragment sample in Figure 4d was measured with the MI SPM at two sensor distances of 14 and 34 mm. The resulting waveforms and their FFT spectrum are provided in Figure 9. The waveform with the longer sensor distance was obviously more sinusoidal than the short distance case, as demonstrated in the FFTs that the contribution from the higher-order harmonics was reduced in the longer distance. The skewness of the waveforms appear to be different from the offset dipole (Figure 7), which could be ascribed to the phase difference between the fundamental wave and the harmonics that may originate from both the irregular sample shape and the magnetization direction.

To test the sensitivity and reproducibility of the MI SPM for samples with weak magnetization, a comparison with a SRM was made using a natural sample: a red shale of 1 inch cylinder with the NRM component normal to the axis that was 3.9×10^{-11} Am^2 and directed 20° in the sample coordinate. The corresponding component was measured with the MI SPM by rotating it about the cylinder axis. Measurements were repeated five times, resulting in the mean direction with magnitude of $4.1 \pm 0.5 \times 10^{-11}$ Am^2 directing $30° \pm 5°$. The magnitude was reasonably in agreement with that by the SRM. The difference in direction appears to be nonnegligible, but might be due to a slight error when repositioning it.

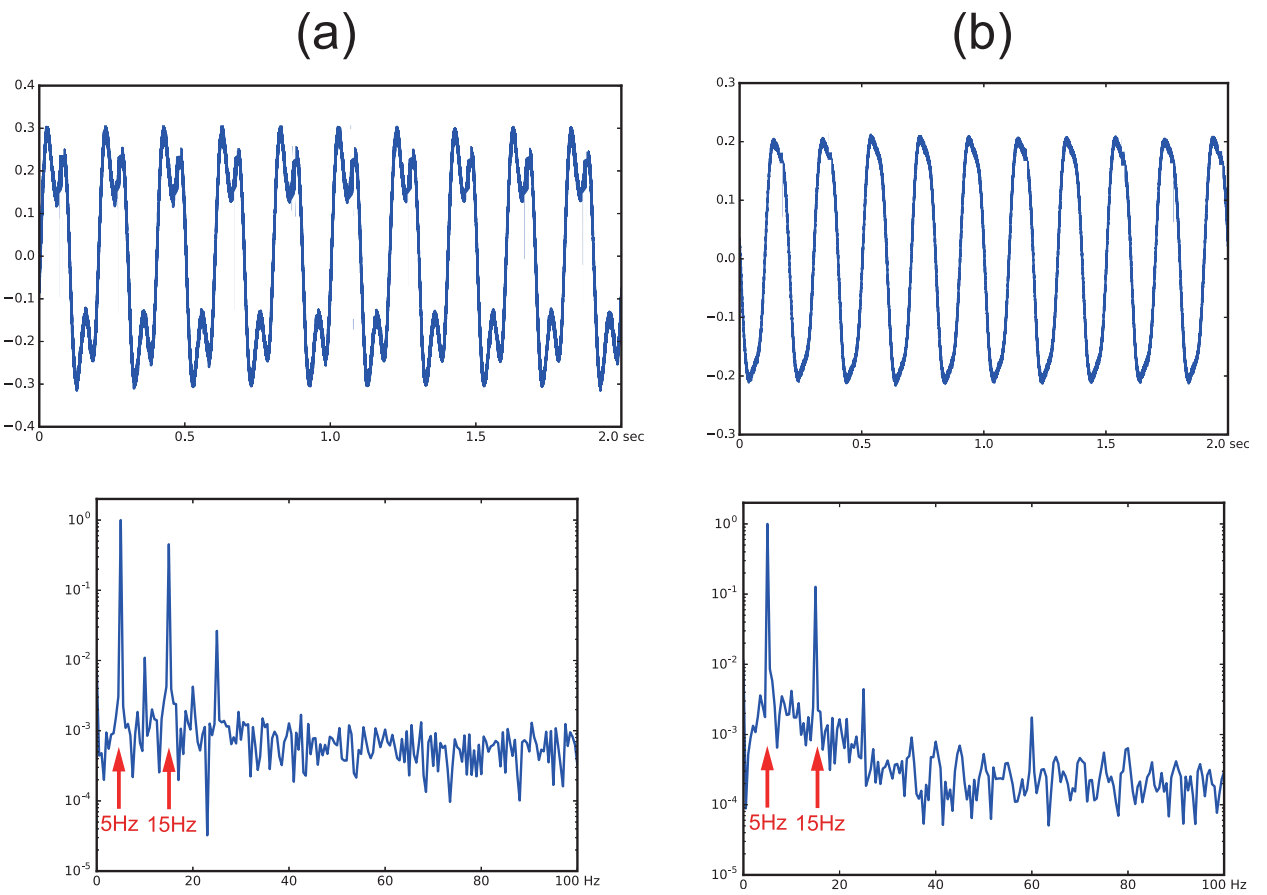

Figure 9. (top) Waveforms and (bottom) their FFT spectrum of the porcelain fragment (Figure 4d), measured at two different sensor distances: (a) 14 mm and (b) 37 mm.

4. Discussion

The measured magnetization of a sample with inhomogeneous magnetization can be described by an offset dipole—an ensemble of a central dipole and other higher-order components [*Irving et al*., 1966; *Collinson*, 1977]. Practically, if samples are in an appropriate shape and measured at a suitable distance from a sensor, the effect of the higher-order magnetic moments should be negligible compared to the nonoffset, central dipole [*Collinson*, 1983]. Thus, it has generally been assumed that the magnetization of natural samples can be represented by a central dipole. However, such a "dipole assumption" would not necessarily hold. For example, in archaeomagnetism, when it is necessary to measure small, irregularly shaped fragments of pottery with an SPM, one might wonder whether the irregularity of the shape could reduce the accuracy of measurements or give rise to systematic errors in the measured magnetization. However, without an objective means to quantify such an effect, one might be unaware of potential errors, and any conclusions drawn might therefore contain a significant amount of error or bias. In such cases, the H mode measurements by the MI spinner would be useful, as exemplified by Figure 9, with the ability to measure the central dipole and other higher-order components and estimate their relative contribution in terms of the FFT spectrum. Based on this objective information, it is possible to exclude samples containing a large number of multipole moments, in addition to central dipoles. Utilizing the additional capability allowing the sensor distance to be flexibly adjusted, it will also be possible to judge the optimum distance at which the higher-order components are sufficiently attenuated, and the magnetization can then be represented only by a central dipole on the basis of the dipole assumption.

The measurement in the H mode is useful for the quantitative estimation of the contributions from the dipole component and higher-order harmonic components. But, it should be noted that generally the harmonic components are observed not only from an offset dipole but also from an inhomogeneously magnetized sample or an irregularly shaped sample. It is expected that the contribution of the harmonics depends

on the degree of the inhomogeneity of such samples in complex manners. Furthermore, if a sample is positioned off the rotating axis of a SPM, the potential effect of the offset will need to be considered. It is to be noted that the measurement in the H mode is not able to distinguish such an inhomogeneously magnetized sample from an offset dipole.

The high sensitivity of the MI SPM is achieved by the capability of sensing magnetic field in closer proximity to a sample than a conventional SPM. This means that the accuracy of the positioning is more critical, which is not necessarily an advantage but a drawback, because small errors in positioning could lead to large measurement errors. But, in other words, combined with a special sample handler allowing precise adjustment of the sensor distance, such as used in this study, it would be possible to determine a critical sensor distance for individual sample, below which it is inappropriate to judge the sample a dipole. Furthermore, how dipolar a sample is could be estimated by plotting the amplitude of the fundamental waves versus the inverse cube of the sensor distance: if the plot turns out to be a straight line, it will be an evidence for the dipolar magnetization, and the gradient of the straight line will represent the intensity of the dipole.

All of the experiments in this study were performed outside the magnetic shield room, and only a one-layer permalloy shield case was used, making the ambient field in the sample-sensor region approximately 1/20 of the surrounding geomagnetic field. The results were compared with those using a three-layer permalloy shield case, but no significant differences were observed in the SNR. One may concern that the nonnegligible ambient field in a weak shield could give rise to an induced magnetization of a sample. However, as described in the previous section, the MI SPM in the H mode measures in principle the fundamental wave and the third-order harmonic, and consequently the possible induced magnetization spun with twice the fundamental frequency is expected to be greatly attenuated. Another advantage of the MI SPM is that the remanence vector of one sample can be obtained by rotating it about two perpendicular axes; for a cylinder sample, one rotation about its axis and the other about the axis normal to it. It is not required, as in conventional SPMs, to change its orientation six times about three orthogonal axes. On the other hand, the high sensitivity of MI SPM that is more strongly dependent of the sensor distance than other SPMs may be a drawback when measuring samples with weak magnetizations. Because it is necessary to measure these samples in close proximity to the sensor, more precise positioning of samples is required.

In conclusion, the MI sensor is sensitive, small-sized, with low power consumption and is therefore most suited for use as the sensor of compact, dynamic magnetometers in order to measure the remanent magnetization.

Acknowledgments

This research was funded by the Monbusho Kakenhi 15H03718 to K.K. Contribution PMG16–01 from the Center for Advanced Marine Core Research, Kochi University. Data measured with the MI SPM can be obtained from the corresponding author (kdma@kochi-u.ac.jp). Hardware design may be obtained from the Natsuhara Giken (natsu@dance.plala.or.jp). Specifications of the MI sensor employed in this study are freely available from the Aichi Micro Intelligent Corporation (http://www.aichi-mi.com/e-home/highly-sensitive-magnetometers/).

References

Bandyopadhyay, S., and M. Cahay (2015), *Introduction to Spintronics*, 2nd ed., CRS Press, Boca Raton, Fla.

Collinson, D. W. (1977), Experiments relating to the measurement of inhomogeneous remanent magnetization in rock samples, *Geophys. J. R. Astron. Soc.*, *48*, 271–275.

Collinson, D. W. (1983), *Methods in Rock Magnetism and Palaeomagnetism*, Chapman and Hall, London.

Dufay, B., S. Saez, C. Dolabdjian, A. Yelon, and D. Ménard (2013), Development of a high sensitivity giant magneto-impedance magnetometer: Comparison with a commercial flux-gate, *IEEE Trans. Magn.*, *49*(1), 85–88, doi:10.1109/TMAG.2012.2219579.

Irving, E., L. Molyneux, and S. K. Runcorn (1966), The analysis of remanent intensities and susceptibilities of rocks, *Geophys. J. Int.*, *10*(5), 451–464, doi:10.1111/j.1365-246X.1966.tb03073.x.

Mohri, K., and Y. Honkura (2007), Amorphous wire and CMOS IC based magneto-impedance sensors–Origin, topics, and future, *Sens. Lett.*, *5*, 267–270, doi:10.1166/sl.2007.082.

Mohri, K., L. V. Panina, T. Uchiyama, M. Noda, and K. Bushida (1995), Sensitive and quick response micromagnetic sensor utilizing magneto-impedance in Co-rich amorphous wires, *IEEE Trans. Magn.*, *31*(2), 1266–1275, doi:10.1109/20.364817.

Mohri, K., M. Fukushima, Y. Mohri, and Yu. Mohri (2010), Detection of magnetization of 6 Hz, 10 μT magnetic field applied water using PT-MI sensor, *PIERS Online*, *6*(2), 145–148, doi:10.2529/PIERS090831112948.

Molyneux, L. (1971), A complete result magnetometer for measuring the remanent magnetization of rocks, *Geophys. J. R. Astron. Soc.*, *24*, 429–433.

Park, J. (2015), Superparamagnetic nanoparticle quantification using a giant magnetoresistive sensor and permanent magnets, *J. Magn. Magn. Mater.*, *389*, 56–60, doi:10.1016/j.jmmm.2015.04.049.

Uchiyama, T., K. Mohri, Y. Honkura, and L. V. Panina (2012), Recent advances of pico-tesla resolution magneto-impedance sensor based on amorphous wire CMOS IC MI sensor, *IEEE Trans. Magn.*, *48*(11), 3833–3839, doi:10.1109/TMAG.2012.2198627.

Uehara, T., and N. Nakamura (2007), Scanning magnetic microscope system utilizing a magneto-impedance sensor for a nondestructive diagnostic tool of geological samples, *Rev. Sci. Instrum.*, *78*, 1–6, doi:10.1063/1.2722402.